Northumbria Research Link

Anisotropic acoustical properties of sintered fibrous metals

H. Meng[1,2], Q.B. Ao[3], S. W. Ren[1,2], F. X. Xin[1,2*], H.P. Tang[3] and T. J. Lu[1,2*]

[1]*Multidisplinary Research Center for Lightweight Structures and Materials, Xi'an Jiaotong University, Xi'an 710049, China*

[2]*State Key Laboratory for Mechanical Structure Strength and Vibration, School of Aerospace, Xi'an Jiaotong University, Xi'an 710049, China*

[3]*State Key Laboratory of Porous Metal Materials, Northwest Institute for Nonferrous Metal Research, Xi'an 710016, China*

A combined theoretical and experimental study is carried out to investigate the anisotropic acoustic properties of sintered fibrous metals. In the theoretical model, based on the transversal and longitudinal dynamic mass densities and effective bulk modulus of randomly placed parallel fibers, the dynamic mass densities and effective dynamic bulk modulus of a sintered fibrous metal in the direction normal and parallel to its surface are obtained. Sound absorption coefficient, sound speed and attenuation coefficient in each of the two directions are calculated once the dynamic mass densities and effective dynamic bulk modulus are determined. For validation, experimental measurements are performed, with good agreement between theoretical prediction and measurement data achieved. Subsequent numerical investigations focus on the influence of fiber diameter and porosity on the anisotropic acoustical properties of the sintered fibrous metal. The sintered fibrous metal exhibits better sound absorption/attenuation performance in the normal direction than in the parallel direction. The anisotropy in acoustical properties increases with decreasing fiber diameter and porosity due mainly to increasing interactions between adjacent fibers.

Keywords: A. Fibres; B. Mechanical properties; C. Anisotropy; D. Acoustic emission

1. Introduction

Fibrous materials are widely applied in the noise control area, either isolated or composited with other structures, for their good sound insulation and absorption ability [1-5]. In particular, fibrous materials made of metal fibers (e.g., stainless steel) through sintering process have promising potential for high-temperature noise control. The present paper aims to investigate theoretically the sound absorption performance of this

---

*Corresponding author. Tel.: +86 29-82663223; fax: +86 29-82663223.
E-mail: fengxian.xin@gmail.com (F.X. Xin) or tjlu@mail.xjtu.edu.cn (T.J. Lu).

kind of fibrous materials, with particular focus placed upon its anisotropic acoustic properties.

A multitude of theoretical models have been proposed to estimate the acoustical properties of fibrous materials. Due to the complex morphology of fibrous materials, one common approach is developing theoretical models based on empirical modeling. For typical instance, Delany and Bazley [6] presented a simple power-law function between the measured characteristic impedance and sound absorption coefficient as well as flow resistivity. Subsequently, Miki [7] and Komatsu [8] modified the Delany-Bazley model for more accurate predictions. Allard and Champoux [9] proposed a new empirical model by taking into account the physical properties of fibrous materials, and found that this model was valid at low frequencies in contrast with the Delany-Bazley model. Other empirical models were also proposed, such as those by Garai and Pompoli [10] and Narang [2] for polyester fibrous materials. In addition to empirical modeling, attempts have also been made to develop theoretical models based on idealized geometry of fibrous materials. For example, Tarnow [11,12] calculated the compressibility and dynamic resistivity by treating the fibrous material as array of periodically arranged parallel fibers, while Dupere *et al.* [13,14] modeled sound propagation both normal and parallel to array of parallel fibers and rigid spheres. Sun *et al.* [15] established that the model of Dupere *et al.* was suitable for sintered fibrous metal materials for high temperature applications. A theoretical model was proposed by Attenborough [16] for rigid fibrous soils and sands, which however needs five physical parameters. Kirby and Cumming [17] presented an improved model based on parallel fiber microstructure, targeting in particular sound absorbing properties at low frequencies.

Although numerous studies have been carried out to explore the acoustical properties of rigid fibrous materials, none concerned the acoustic anisotropy of fibrous materials. In the present study, a combined theoretical and experimental approach is employed to reveal the anisotropic acoustical properties of sintered fibrous metals. First, the dynamic mass density (i. e. the ratio of the pressure gradient to the averaged fluid acceleration) and effective bulk modulus (i. e. the ratio of the pressure increase to the decrease of relative volume) for sound propagating normal and parallel to randomly placed parallel fibers are calculated theoretically to estimate the dynamic mass density and effective

bulk modulus of a sintered fibrous metal along both parallel and normal directions. Next, the validity of the model predictions is checked against experimental measurements, with good agreement achieved. The model is subsequently used to analyze the acoustic anisotropy of the material in terms of sound absorption coefficient, sound speed and attenuation coefficient. The influence of fiber diameter and porosity on the acoustic anisotropy is quantified.

2. Theoretical model

Consider a sintered fibrous metal as shown in Fig. 1. As the metal fibers having equal diameter ($\sim 50\,\mu m$) randomly lie in parallel planes, the fibrous metal may be regarded as a transversely isotropic material. In the present study, for convenience, the plane parallel to all the fibers is referred to as the "fiber plane". With reference to Figs. 1(a) and (b), the acoustical properties of the sintered fibrous metal in the direction normal to the fiber plane are expected to be different from those in the direction parallel to it. Since the stiffness and density of the metal fibers are much larger than that of the fluid (air in the current study) saturated in the fibrous metal, the fibers are regarded as rigid bodies.

The dynamic mass densities of the sintered fibrous metal in different directions are calculated based on the array of randomly placed parallel fibers as shown in Fig. 2(a). The dash lines marked around the fibers are called Voronoi polygons, which represent the interaction of adjacent fibers in the parallel fiber array. For simplicity, each Voronoi polygon is approximated by a circle having the same area; see Fig. 2(b). The porosity of the parallel fiber array is identical to that of the considered sintered fibrous metal.

Consider first sound propagating parallel to the parallel fiber array, namely, parallel to the z-direction of Fig. 2. Since the void space among these fibers is small, the viscosity of the saturated fluid is significant and should be taken into account in acoustic modeling. The fluid motion is governed by the viscous Navier-Stokes equation, as:

$$\nabla^2 u_z - \frac{i\omega\rho_0}{\eta} u_z = \frac{1}{\eta}\frac{\partial p}{\partial z} \tag{1}$$

where u_z is the fluid velocity in the z-direction, ω is the angular frequency, η denotes the dynamic viscosity, p is the fluid pressure and ρ_0 is the fluid density. By

approximating the Voronoi polygons by circles having the same area [12], the general solution for Eq. (1) can be written in the form [18]:

$$u_z(r) = A_0 Ke_0\left(\sqrt{\frac{\omega}{v}}r\right) + B_0 Be_0\left(\sqrt{\frac{\omega}{v}}r\right) - \frac{1}{i\rho\omega}\frac{\partial p}{\partial z} \tag{2}$$

where $Ke_m(x) = ker_m(x) + ikei_m(x), Be_m(x) = ber_m(x) + ibei_m(x)$, ker_m, kei_m, ber_m, bei_m are the Kelvin functions, (r,θ) are the polar coordinates (Fig. 2), and A_0 and B_0 are unknown coefficients to be determined by applying relevant boundary conditions.

Due to the viscosity of the fluid, the velocity at the interface between the fluid and the fiber is zero:

$$u_z(r,\theta)\big|_{r=a} = 0 \tag{3}$$

where a is the fiber radius. Besides, no shear stresses exist on the outer boundaries of the fibers, therefore, for a circle with radius r_{out}, the boundary condition is [13]:

$$\frac{\partial u_z}{\partial r}\bigg|_{r=r_{out}} = 0 \tag{4}$$

Upon substitution of Eq. (2) into Eqs. (3) and (4), the coefficients A_0 and B_0 are obtained as:

$$A_0 = \frac{1}{Ke_0(R_0) - \dfrac{Ke_1(R_1)}{Be_1(R_1)}Be_0(R_0)}\frac{1}{\rho i\omega}\frac{\partial p}{\partial z} \tag{5}$$

$$B_0 = \frac{-1}{Ke_0(R_0) - \dfrac{Ke_1(R_1)}{Be_1(R_1)}Be_0(R_0)}\frac{Ke_1(R_1)}{Be_1(R_1)}\frac{1}{\rho i\omega}\frac{\partial p}{\partial z} \tag{6}$$

The velocity u_z is determined by substituting Eqs. (5) and (6) into Eq. (2), from which the mean velocity $\bar{u}_z$ is calculated as:

$$\bar{u}_z(r_{out},\omega) = \frac{1}{S}\iint_S u_z(r)\,dS = \frac{1}{\pi r_{out}^2 - \pi a^2}\int_a^{r_{out}} u_z(r)2\pi r\,dr \tag{7}$$

where $S = \pi r_{out}^2 - \pi a^2$ is the area occupied by the fluid in one cell.

For the parallel fiber array of Fig. 2(a), the Voronoi polygon with area S has a probability $p(S)dS$ in the interval between S and $S+dS$ [12]:

$$p(S) = \frac{1}{\overline{S}} \frac{\alpha^\alpha}{\Gamma(\alpha)} \left(\frac{S}{\overline{S}}\right)^{\alpha-1} \exp\left(-\alpha \frac{S}{\overline{S}}\right) \tag{8}$$

where $\Gamma(\alpha)$ is the gamma function with $\alpha = 3.61$, $\overline{S} = \frac{\pi a^2}{1-\Omega}$ is the mean area of the polygons for parallel fibers, and Ω is the porosity (i. e. the fraction of the volume of voids over the total volume) of the parallel fiber array. Therefore, with the random distribution of fibers accounted for, the mean velocity of fluid flow in the z-direction is

$$\bar{u}_z'(\omega) = \int_S \bar{u}_z(r_{out}, \omega) p(S) dS = \int_a^\infty \bar{u}_z(r_{out}, \omega) p(\pi r_{out}^2) 2\pi r_{out} dr_{out} \tag{9}$$

Finally, the longitudinal (z-direction) dynamic mass density of the parallel fiber array is obtained as:

$$\rho_\parallel(\omega) = \frac{-1}{i\omega} \frac{\partial p}{\partial z} \frac{1}{\bar{u}_z'(\omega)} \tag{10}$$

For sound propagating normal to the fiber axis (i.e., x-direction in Fig. 2), the fluid velocity is governed by the viscous Navier-Stokes equation as:

$$\nabla^2 \mathbf{u} - \frac{i\omega\rho_0}{\eta} \mathbf{u} = \frac{1}{\eta} \frac{\partial p}{\partial x} \tag{11}$$

where $\mathbf{u}(r, \theta)$ is the fluid velocity vector, which has two components, u_r and u_θ, in the (r, θ) polar coordinates (Fig. 2). The velocity should be zero on the fiber surface, yielding:

$$\mathbf{u}(r, \theta)\big|_{r=a} = 0 \tag{12}$$

Also, the vorticity should be zero on the outer boundary [13]:

$$\mathrm{curl}\,\mathbf{u}\big|_{r=r_{out}} = 0 \tag{13}$$

From Eqs. (11), (12) and (13), the fluid velocity can be obtained as [13]:

$$u_r = \left[\frac{Ke_1(R_0) - R_0 Ke_1'(R_0)}{Ke_1(R_0) + R_0 Ke_1'(R_0)} \left(\frac{a^2}{r^2} \right) + 1 - \frac{2(a/r) Ke_1\left(\sqrt{\frac{\omega \rho_0}{\eta}} r \right)}{Ke_1(R_0) + R_0 Ke_1'(R_0)} \right] \frac{\partial p}{\partial x} \frac{-1}{i\omega \rho_0} \cos\theta e^{i\omega t}$$

$$u_\theta = \left[\frac{Ke_1(R_0) - R_0 Ke_1'(R_0)}{Ke_1(R_0) + R_0 Ke_1'(R_0)} \left(\frac{a^2}{r^2} \right) - 1 + \frac{2 \sqrt{\frac{\omega \rho_0}{\eta}} a Ke_1'\left(\sqrt{\frac{\omega \rho_0}{\eta}} r \right)}{Ke_1(R_0) + R_0 Ke_1'(R_0)} \right] \frac{\partial p}{\partial x} \frac{-1}{i\omega \rho_0} \sin\theta e^{i\omega t}$$

(14)

where $R_0 = \sqrt{\frac{\omega \rho_0}{\eta}} a$. The mean velocity in the x-direction can thence be calculated as:

$$\bar{u}_x(r_{out}, \omega) = \frac{1}{S} \iint_S u_x r dr d\theta = \frac{1}{\pi(r_{out}^2 - a^2)} \int_0^{2\pi} \int_a^{r_{out}} (u_r \cos\theta - u_\theta \sin\theta) r dr d\theta \qquad (15)$$

Further, given the random distribution of the parallel fibers, the mean velocity in the x-direction is given by:

$$\bar{u}_x'(\omega) = \int_S \bar{u}_x(r_{out}, \omega) p(S) dS = \int_a^\infty \bar{u}_x(r_{out}, \omega) p(\pi r_{out}^2) 2\pi r_{out} dr_{out} \qquad (16)$$

Finally, the transversal dynamic mass density of the parallel fiber array is calculated as:

$$\rho_\perp(\omega) = \frac{-1}{i\omega} \frac{\partial p}{\partial x} \frac{1}{\bar{u}_x'(\omega)} \qquad (17)$$

Next, to calculate the effective bulk modulus of the sintered fibrous metal, the distribution of temperature in the parallel fiber array of Fig. 2 should be obtained. The temperature distribution is independent of sound propagation direction, governed by the thermal conduction equation as [19]:

$$k_t \nabla^2 T(r, \omega) - i\omega \rho_0 c_p T(r, \omega) = -i\omega P(\omega) \qquad (18)$$

where $T(r, \omega)$ is the temperature rise, $P(\omega)$ is the pressure rise, k_t is the thermal conductivity of the fluid, and c_p is the specific heat per unit mass at constant pressure.

With isothermal condition assumed, the temperature rise at the fiber surface is zero:

$$T(r, \omega)\big|_{r=a} = 0 \qquad (19)$$

The thermal flux should also be zero on the outer boundary. For a circular boundary with radius r_{out}, this becomes:

$$\left.\frac{\partial T(r,\omega)}{\partial r}\right|_{r=r_{out}} = 0 \tag{20}$$

Due to the similarity between Eqs. (1) and (18), the solution of temperature rise can be expressed by using the velocity solution of Eq. (1). The mean velocity $\bar{u}_z'(\omega)$ can be expressed as $\bar{u}_z'(\omega) = \frac{-1}{\rho i \omega}\frac{\partial p}{\partial z}\varphi(\omega)$, then the mean temperature rise can be given by:

$$\bar{T}'(\omega) = \frac{P(\omega)}{\rho_0 c_p}\varphi(\mathrm{Pr}\,\omega) \tag{21}$$

where $\mathrm{Pr} = c_p \eta / k_t$ is the Prandtl number. Correspondingly, the effective bulk modulus is calculated as:

$$K_{eff} = \frac{P(\omega)}{\mathrm{d}\rho/\rho_0} = \frac{\gamma P_0}{\gamma - (\gamma-1)\dfrac{\rho_0 c_p}{P}\bar{T}'(\omega)} \tag{22}$$

where γ is the specific heat ratio of the fluid, P_0 is the static pressure of air, and according to the state equation of air, $\mathrm{d}\rho/\rho_0 = P(\omega)/P_0 - \bar{T}'(\omega)/T_0$.

As shown in Fig. 1, when a sound wave propagates normal to the fiber plane, the sound is perpendicular to all the fibers in the fibrous metal. Therefore, the dynamic mass density of the fibrous metal may be approximated by the transversal dynamic mass density of the parallel fiber array, as:

$$\rho_N \approx \rho_\perp \tag{23}$$

In reality, as the fibers are not parallel but overlapped in the fibrous metal as shown in Fig. 1, a modified factor considering the microstructure of the fibrous material is added to the dynamic mass density, yielding:

$$\rho_N' \approx m_N \rho_N \tag{24}$$

where m_N is assumed equal to the square root of the tortuosity of the sintered fibrous metal in the direction normal to the fiber plane. Depending upon the microstructure of the fibrous metal, the tortuosity may be obtained by applying the self-consistent approximation method. Thus, in the direction normal to the fiber plane, the tortuosity is determined by [20]:

$$\alpha_{\infty N} = \left(\frac{c_0}{c_N(\omega)} \right)^2 \Bigg|_{\omega \to \infty} \tag{25}$$

where $c_N(\omega)$ is the sound speed in the fibrous metal in the direction normal to the fiber plane. This sound speed can be estimated by:

$$c_N(\omega) = \frac{\omega}{\mathrm{Re}(k_N(\omega))} \tag{26}$$

where $k_N(\omega)$ is the complex wave number in the fibrous material, given by:

$$k_N(\omega) = \omega \sqrt{\frac{\rho'_N(\omega)}{K_{eff}(\omega)}} \tag{27}$$

Therefore, the tortuosity in the direction normal to the fiber plane can be written as:

$$\alpha_{\infty N} = \mathrm{Re}\left(\frac{\rho'_N(\omega)}{K_{eff}(\omega)} \right) c_0^{\,2} \Bigg|_{\omega \to \infty} \tag{28}$$

Equations (24) and (28) are solved by an iterative process. First, a value for $\alpha_{\infty N}$ is chosen, for example $\alpha_{\infty N} = 1.5$, then the corresponding value of the dynamic mass density ρ'_N is computed by (24). Based on this value of ρ'_N, a new value of $\alpha_{\infty N}$ is obtained by (28) from which a new value of ρ'_N is calculated. This iteration process is repeated until a stable value of $\alpha_{\infty N}$ is obtained.

It has been established that the in-plane permeability of two-dimensional (2D) cross-plies and 2D randomly overlapping fiber structures is close to the averaged value of the transversal and longitudinal permeabilities of parallel fiber arrays [21,22]. As the dynamic mass density is inversely proportional to the permeability, in the present study, the averaged value of the transversal and longitudinal dynamic mass densities of the parallel fiber array is employed to approximate the dynamic mass density of the sintered fibrous material in the direction parallel to the fiber plane:

$$\rho_P \approx \frac{\rho_{\parallel} + \rho_{\perp}}{2} \tag{29}$$

Further, due to the complex architecture of the sintered fibrous metal (see Fig. 1), the concept of modified factor is applied to calculate more accurately the dynamic mass density in the direction parallel to the fiber plane, as:

$$\rho_P' \approx m_P \rho_P \tag{30}$$

where m_P is the modified factor that is equal to the square of tortuosity in the direction parallel to the fiber plane. Similar to the above iterative process for $\alpha_{\infty N}$, m_P can also be determined using the self-consistent approximation approach.

Once the dynamic mass densities ρ_P' and ρ_N' as well as the effective bulk modulus K_{eff} are known, the wavenumbers (k_P, k_N) and the characteristic impedances (Z_P, Z_N) for sound propagation parallel and normal to the fiber plane can be obtained as:

$$Z_P = \sqrt{\rho_P' K_{eff}}, \; Z_N = \sqrt{\rho_N' K_{eff}} \tag{31}$$

$$k_P = \omega \sqrt{\frac{\rho_P'}{K_{eff}}}, \; k_N = \omega \sqrt{\frac{\rho_N'}{K_{eff}}} \tag{32}$$

Correspondingly, the sound speed and attenuation in the two directions are given by:

$$c_N = \frac{\omega}{\mathrm{Re}(k_N)}, \; c_P = \frac{\omega}{\mathrm{Re}(k_P)} \tag{33}$$

$$\delta_N = -\mathrm{Im}(k_N), \; \delta_P = -\mathrm{Im}(k_P)$$

For a rigid-backed sintered fibrous metal sample with its surface normal to the fiber plane, its sound absorption coefficient for normal incident sound is:

$$\alpha_N = 1 - \left| \frac{Z_{sN} - \rho_0 c_0}{Z_{sN} + \rho_0 c_0} \right|^2 \tag{34}$$

where $Z_{sN} = -i Z_N \cot(k_N d_N)$ is the surface impedance of the sample and d_N is the thickness of the sample.

Similarly, for a rigid-backed sintered fibrous metal sample with its surface parallel to the fiber plane, its sound absorption coefficient for normal incident sound is:

$$\alpha_P = 1 - \left| \frac{Z_{sP} - \rho_0 c_0}{Z_{sP} + \rho_0 c_0} \right|^2 \tag{35}$$

where $Z_{sP} = -i Z_P \cot(k_P d_P)$ is the surface impedance of the sample and d_P is the thickness of the sample.

3. Experimental measurements

The proposed theoretical model for sound propagation in sintered fibrous metals is

validated against experimental measurement results. The sound absorption coefficients of sintered fibrous metal samples (Fig. 3) are measured in the B&K 4206 impedance tube by applying the transfer function method. The tested sample is mounted at one end of the tube, while plane sound waves are generated at the other end of the impedance tube. The sound pressures in the impedance tube are measured by two wall-mounted microphones at two fixed locations. The reflection coefficient and sound absorption coefficient can then be calculated by the measured sound pressures [23]. In total, four groups of sintered fibrous metal samples having the same porosity (90%) and fiber diameter ($50\,\mu m$) are measured. From group to group, the thickness of the samples varies as 20 mm, 27 mm, 35 mm and 57 mm. As shown in Fig. 4, each group contains two different kinds of samples. The surface of one kind of sample is parallel to the fiber plane, while the surface of the other is normal to it. The physical parameters of the test samples are listed in Table 1. In the present study, the sintered fibrous metal is manufactured using randomly distributed stainless steel fibers of different length (10 mm~ 50 mm) but same diameter which are bonded to constitute a whole sample via furnace sintering. Thus the fiber diameter is known in the manufacturing process, while the porosity of the sample is obtained by comparing its density with that of the fibers.

The experimentally measured and theoretically predicted sound absorption coefficients are compared in Fig. 5 for all the four groups of sintered fibrous metal samples. The theoretical curves exhibit the same trends as those of the measured ones, capturing in particular all the peaks and dips. The discrepancies between the experimental and theoretical results may be attributed to the idealized handling of the connections between the fibers in the theoretical model. It can also be seen from Fig. 5 that the samples with incident surfaces parallel to the fiber plane always have a bigger sound absorption coefficient than that with incident surface normal to the fiber plane. In order to explain this trend, the sound speed and attenuation of sintered fibrous metals predicted using the theoretical model for sound incidence parallel and normal to the fiber plane are compared in Fig. 6.

As shown in Fig. 6, the speed of sound propagation parallel to the fiber plane is smaller than that normal to it at low frequencies, approaching the latter as the frequency exceeds about 1000 Hz. Correspondingly, within the considered frequency range, the attenuation of sound propagation parallel to the fiber plane is bigger than that normal to

it. Together with the sound absorption comparison in Fig. 5, the present results demonstrate that the sound absorption ability of the sintered fibrous metal is better in the direction parallel to the fiber plane than that in the direction normal to it.

4. Anisotropic acoustic properties of sintered fibrous metal

In this section, the proposed theoretical model, validated against experimental measurements, is employed to investigate the effects of morphological parameters (fiber diameter and porosity in particular) of the sintered fibrous metal on its anisotropic acoustical properties. A more fundamental understanding on sound propagation in this kind of materials is provided.

4.1 Influence of fiber diameter

Figure 7 plots the predicted sound absorption coefficient of rigid-backed sintered fibrous stainless steel sheet as a function of frequency for three different fiber diameters, 40 μm, 50 μm and 60 μm, both for sound propagating normal and parallel to the fiber plane. For the plotting, the porosity and sheet thickness are fixed at 90% and 20 mm, respectively. It can be seen from Fig. 7 that the sound absorption coefficient increases as the fiber diameter is decreased. For the cell shown in Fig. 2(b), the specific contact area between the saturated fluid and fibers in the fibrous metal is:

$$S_c = \frac{2(1-\Omega)}{a} \tag{36}$$

The specific contact area (SCA) is the contact area between the fluid and fibers in unit volume of the material. It can be deduced from (36) that the specific contact area between the fluid and fibers grows as the fiber diameter decreases for a given porosity. The viscous effect is intensified as the specific contact area is increased, beneficial for enhanced sound absorption.

Figure 8 plots the sound speed and attenuation coefficient as functions of frequency for selected fiber diameters (porosity 90% and sheet thickness 20 mm). The results of Fig. 8 show that the sound speed decreases while the attenuation coefficient increases with decreasing fiber diameter. These trends can also be attributed to the increased viscous effect as the fiber diameter is decreased. Figures 7 and 8 also reveal the difference in acoustical properties between normal and parallel incidence when the fiber diameter is varied. Here we define three parameters to represent the difference in

acoustical properties:

Sound absorption difference:

$$\chi_\alpha(\omega) = \frac{\left|\alpha_P(\omega) - \alpha_N(\omega)\right|}{\alpha_P(\omega)} \qquad (37)$$

Sound speed difference:

$$\chi_{sp}(\omega) = \frac{\left|c_P(\omega) - c_N(\omega)\right|}{c_P(\omega)} \qquad (38)$$

Attenuation difference:

$$\chi_{at}(\omega) = \frac{\left|\delta_P(\omega) - \delta_N(\omega)\right|}{\delta_P(\omega)} \qquad (39)$$

The sound absorption difference (SAD), sound speed difference (SPD) and attenuation difference (AD) is able to characterize the relative differences of the acoustic properties in the two principle directions of sintered fibrous metals. It can be seen from Fig. 9 that the acoustical property differences all decrease as the fiber diameter is increased, implying that the acoustic anisotropy of the sintered fibrous metal is weakened by increasing the fiber diameter. As the fiber diameter is increased while the porosity is fixed, the space between the fibers is enlarged, which weakens the interaction among the fibers. Therefore, fiber distribution plays a less important role in the acoustical properties of the sintered fibrous metal.

4.2 Influence of porosity

Figure 10 plots the predicted sound absorption coefficient of rigid-backed sintered fibrous stainless steel sheet as a function of frequency for three different porosities, 0.8, 0.85 and 0.9, both for sound propagating normal and parallel to the fiber plane. The fiber diameter and sheet thickness are fixed at 50 μm and 20 mm, respectively. As the porosity is decreased, the sound absorption coefficient curve shifts to lower frequency as a whole. This can be explained by comparing the sound speeds calculated with different porosities shown in Fig. 11(a). As is known, the sound absorption peak appears when the distance between the incidence and reflected sound is equal to 1/4 wavelength, namely:

$$d = \frac{1}{4}\lambda_p = \frac{1}{4}\frac{c}{f_p} \tag{40}$$

where λ_p is the wavelength of sound at the peak frequency f_p, and c is sound speed in the fibrous metal. From Fig. 11(a) it is seen that the sound speed decreases with decreasing porosity, causing reduced peak frequency. In addition, Fig. 11(b) presents the variation trend of the attenuation coefficient with porosity. The attenuation coefficient decreases as the porosity is increased. As shown in Eq. (36), the specific contact area decreases with increasing porosity and fixed fiber diameter, weakening therefore the viscous effect. Correspondingly, the sound speed increases while the attenuation coefficient decreases.

It can be seen from Fig. 12 that the difference in acoustical properties shown in Figs. 10 and 11 decreases in general with increasing porosity except that the difference in sound speed fluctuates in the high frequency range (> 1500 Hz). As the porosity is increased, the space between adjacent fibers is enlarged. As aforementioned, the acoustic anisotropy of the sintered fibrous metal is weakened as the space between fibers is increased. Given that the sound absorption peaks at quarter-wavelength resonance, it is thus understandable for the fluctuation appearing in Fig. 12(a).

5. Conclusions

The anisotropic acoustical properties of sintered fibrous metal (stainless steel) are investigated both theoretically and experimentally. Built upon the idealized model of randomly placed parallel fiber array, the dynamic mass density and effective bulk modulus of sound propagation both normal and parallel to the fiber plane are calculated by solving the velocity and temperature fields in the array. Acoustical properties including sound absorption, sound speed and attenuation coefficient of sintered fibrous metal sheets are obtained as functions of morphological parameters such as porosity, fiber diameter and sheet thickness. Experimental measurements are carried out to validate the theoretical model predictions, with good agreement achieved. The model is subsequently employed to quantify the influence of fiber diameter and porosity on the acoustic anisotropy of the sintered fibrous metal. The main findings are summarized as follows:

1) As the fiber diameter (other relevant parameters fixed) is decreased, the sound

absorption coefficient of sintered fibrous metal increases due mainly to enhanced viscous effect,

2) The sound absorption coefficient decreases with increasing porosity (other relevant parameters fixed) due to shift of sound absorption peak towards low frequency.

3) The sintered fibrous metal exhibits anisotropic acoustical properties, having higher sound absorption/attenuation coefficient and lower sound speed in the direction parallel to the fiber plane than those in the direction normal to it. The difference in acoustic properties between parallel and normal directions decreases with increasing fiber diameter or increasing porosity due to reduced fiber distribution effect (i.e., fiber interaction effect).

Acknowledgement

References

[1] AL-Rahman LA, Raja RI, Rahman RA. Attenuation of noise by using absorption materials and barriers: a review. Int J Eng Tech. 2012;2(7):1207-1217.

[2] Narang P. Material parameter selection in polyester fiber insulation for sound transmission and absorption. Appl Acoust. 1995;45(4):335-358.

[3] Meng H, Xin FX, Lu TJ. External mean flow effects on sound transmission through acoustic absorptive sandwich structure. AIAA J. 2012;50(10):2268-2276.

[4] Lee I, Selamet A, Huff NT. Acoustic impedance of perforations in contact with fibrous material. J Acoust Soc Am. 2006;119(5):2785-2797.

[5] Arenas JP, Crocker MJ. Recent trends in porous sound-absorbing materials. J Sound Vib. 2010;44(7):12-18.

[6] Delany ME, Bazley EN. Acoustical properties of fibrous absorbent materials. Appl Acoust. 1970;3(2):105-116.

[7] Miki Y. Acoustical properties of porous materials-Modifications of Delany-Bazley models. J Acoust Soc Jap (E). 1990;11(1):19-24.

[8] Komatsu T. Improvement of the Delany-Bazley and Miki models for fibrous sound-absorbing materials. Acoust Sci Tech. 2008;29(2):121-129.

[9] Allard JF, Champoux Y. New empirical equations for sound propagation in rigid frame

fibrous materials. J Acoust Soc Am. 1992;91(6):3346-3353.

[10] Garai M, Pompoli F. A simple empirical model of polyester fibre materials for acoustical applications. Appl Acoust. 2005;66(12):1383-1398.

[11] Tarnow V. Compressibility of air in fibrous materials. J Acoust Soc Am. 1996;99(5):3010-3017.

[12] Tarnow V. Calculation of the dynamic air flow resistivity of fiber materials. J Acoust Soc Am. 1997;102(3):1680-1688.

[13] Dupère ID, Dowling AP, Lu TJ. The absorption of sound in cellular foams. ASME International Mechanical Energineering Congress. California, November, 2004.

[14] Dupere ID, Lu T, Dowling A. Optimization of cell structures of cellular materials for acoustic applications. Proceedings of 12th International Congress on Sound and Vibration (ICSV12). Lisbon, July, 2005. p. 329.

[15] Sun F, Chen H, Wu J, Feng K. Sound absorbing characteristics of fibrous metal materials at high temperatures. Appl Acoust. 2010;71(3):221-235.

[16] Attenborough K. Acoustical characteristics of rigid fibrous absorbents and granular materials. J Acoust Soc Am. 1983;73(3):785-799.

[17] Kirby R, Cummings A. Prediction of the bulk acoustic properties of fibrous materials at low frequencies. Appl Acoust. 1999;56(2):101-125.

[18] Umnova O, Tsiklauri D, Venegas R. Effect of boundary slip on the acoustical properties of microfibrous materials. J Acoust Soc Am. 2009;126(4):1850-1861.

[19] Zhang B, Chen T. Calculation of sound absorption characteristics of porous sintered fiber metal. Appl Acoust. 2009;70(2):337-346.

[20] Umnova O, Attenborough K, Shin H-C, Cummings A. Deduction of tortuosity and porosity from acoustic reflection and transmission measurements on thick samples of rigid-porous materials. Appl Acoust. 2005;66(6):607-624.

[21] Liu HL, Hwang WR. Permeability prediction of fibrous porous media with complex 3D architectures. Compos Part A. 2012;43(11):2030-2038.

[22] Tomadakis MM, Robertson TJ. Viscous permeability of random fiber structures: comparison of electrical and diffusional estimates with experimental and analytical results. J Compos Mater. 2005;39(2):163-188.

[23] ISO 10534-2-1998. Acoustics determination of sound absorption coefficient and impedance in impedance tubes - Part 2: Transfer-function method.
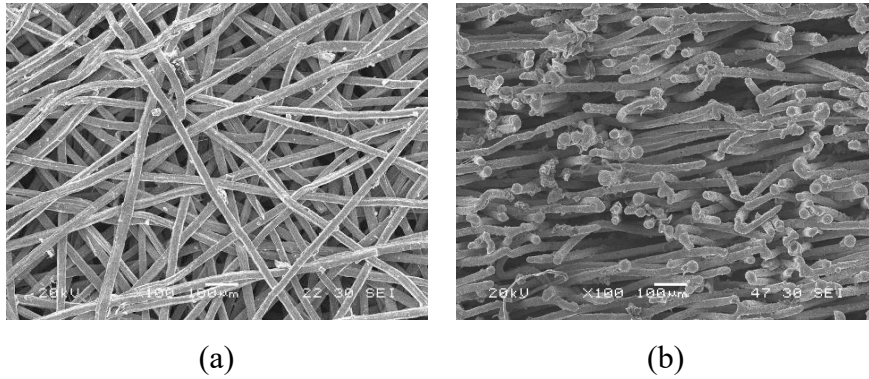
List of figures

(a)   (b)

Fig.1 Photographs of sintered fibrous metal: (a) surface parallel to fiber plane; (b) surface normal to fiber plane.
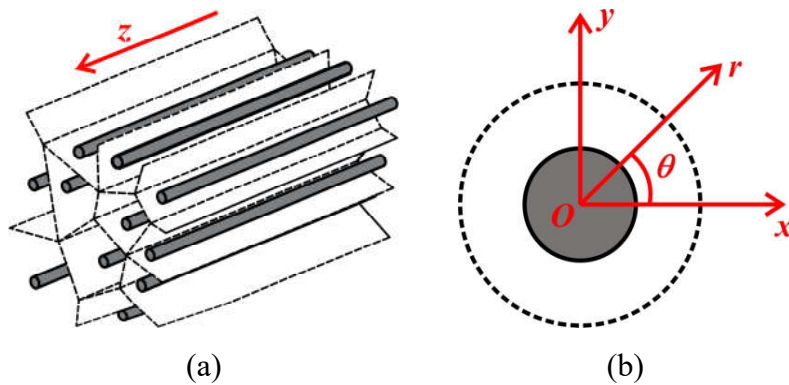

(a)   (b)

Fig. 2 (a) Schematic illustration of parallel fiber array with Voronoi outer boundaries; (b) cross section of one cell with approximated circular outer boundary
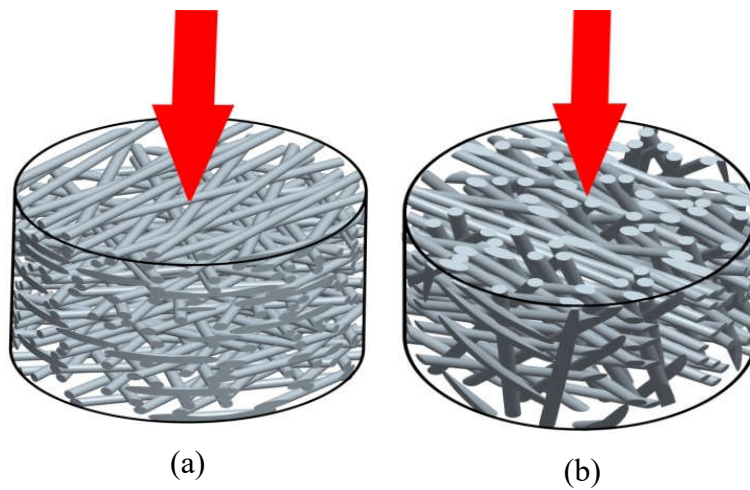
Fig. 3 Test samples of sintered fibrous metal

| (a) | (b) |

Fig. 4 Schematic illustration of sintered fibrous metal: (a) sound incidence normal to fiber plane; (b) sound incidence parallel to fiber plane
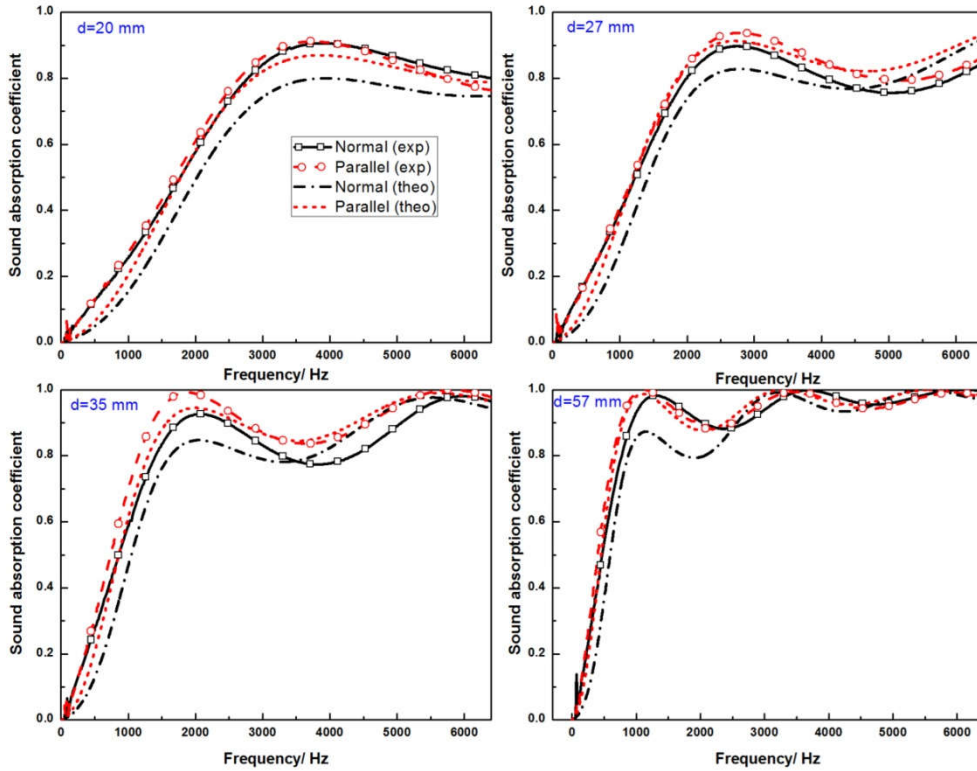
Fig. 5 Comparison between experimental measurements and model predictions for sound absorption of rigid-backed sintered fibrous stainless steel samples having different thicknesses
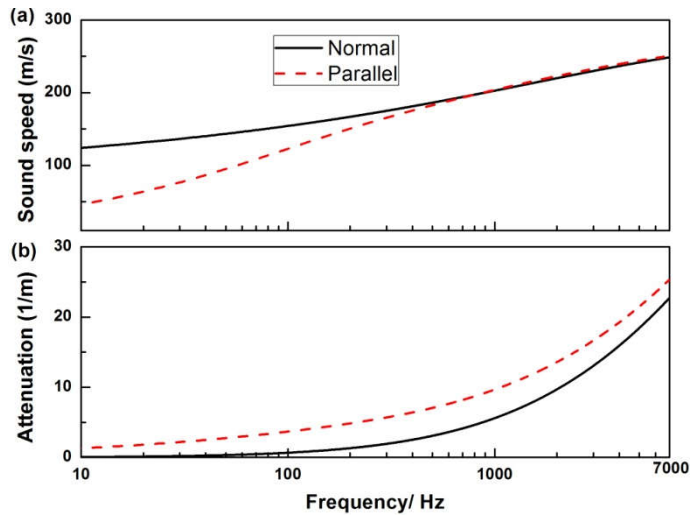
Fig. 6 Sound speed and attenuation coefficient of sintered fibrous metal for sound incidence parallel and normal to the fiber plane
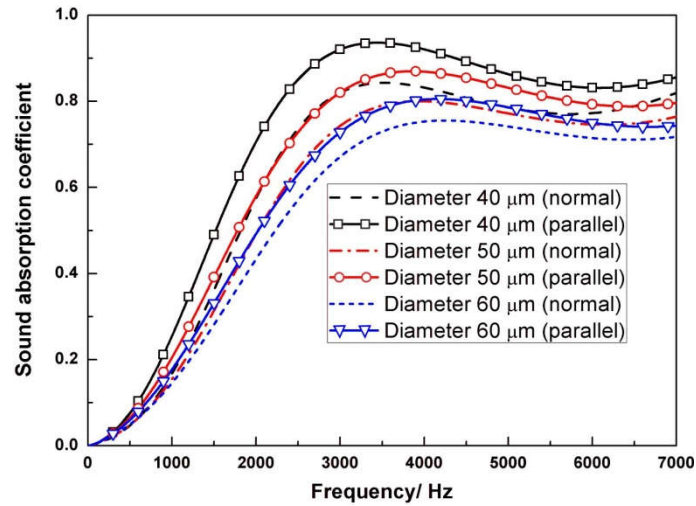
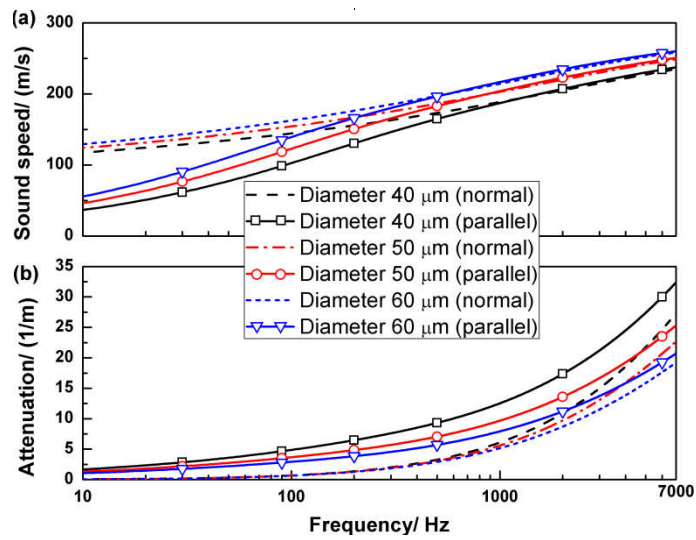**Fig. 7** Sound absorption coefficient of sintered fibrous metal sheet for selected fiber diameters with fixed porosity of 90% and sheet thickness of 20 mm

Fig. 8 Sound speed and attenuation coefficient of sintered fibrous metal sheet for selected fiber diameters with fixed porosity of 90% and sheet thickness of 20 mm
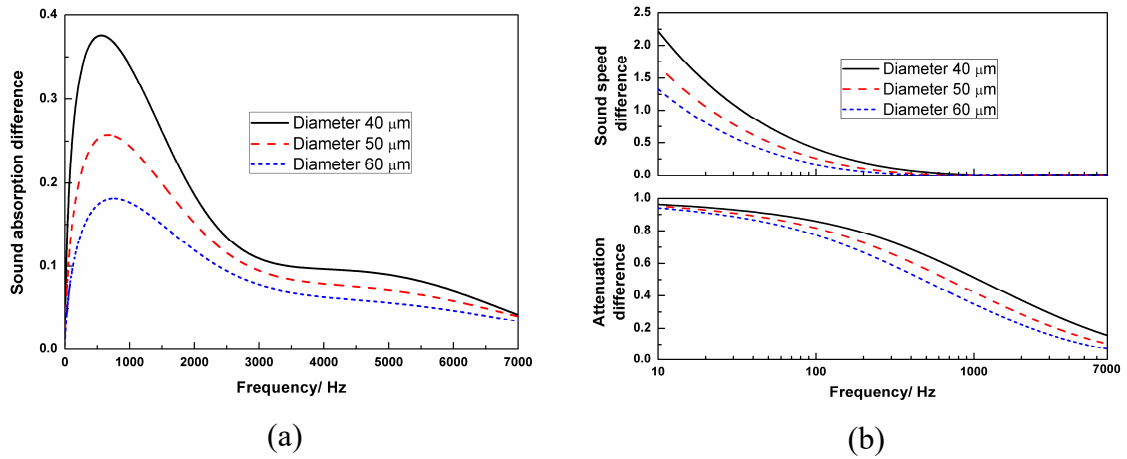
(a)   (b)

Fig. 9 Anisotropic acoustic properties of sintered fibrous metal sheet for selected fiber diameters (porosity 90% and sheet thickness 20 mm): (a) sound absorption difference; (b) sound speed and attenuation differences
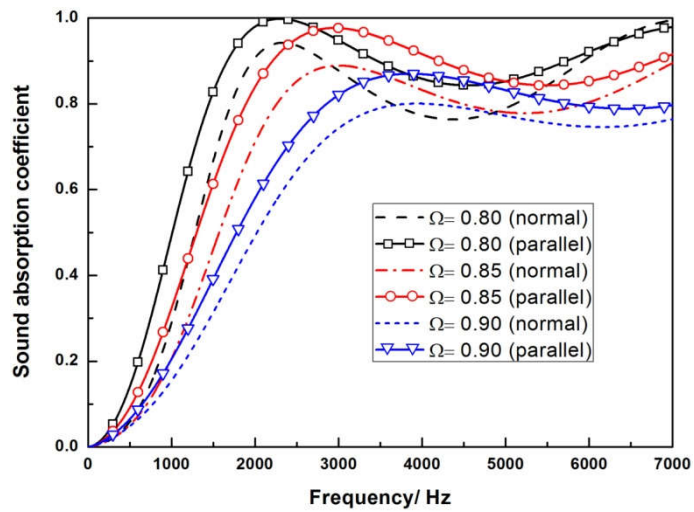

Fig. 10 Sound absorption coefficient of sintered fibrous metal sheet for selected porosities with fixed fiber diameter of 50 μm and sheet thickness of 20 mm
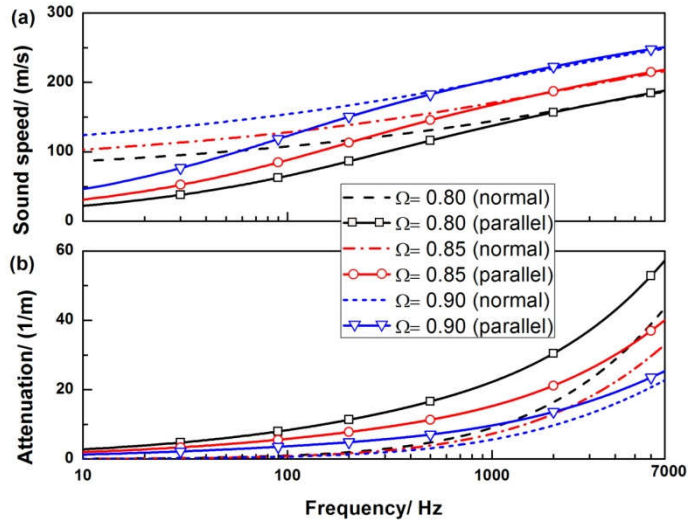
Fig. 11 Sound speed and attenuation coefficient of sintered fibrous metal sheet for selected porosities with fixed fiber diameter of 50 μm and sheet thickness of 20 mm
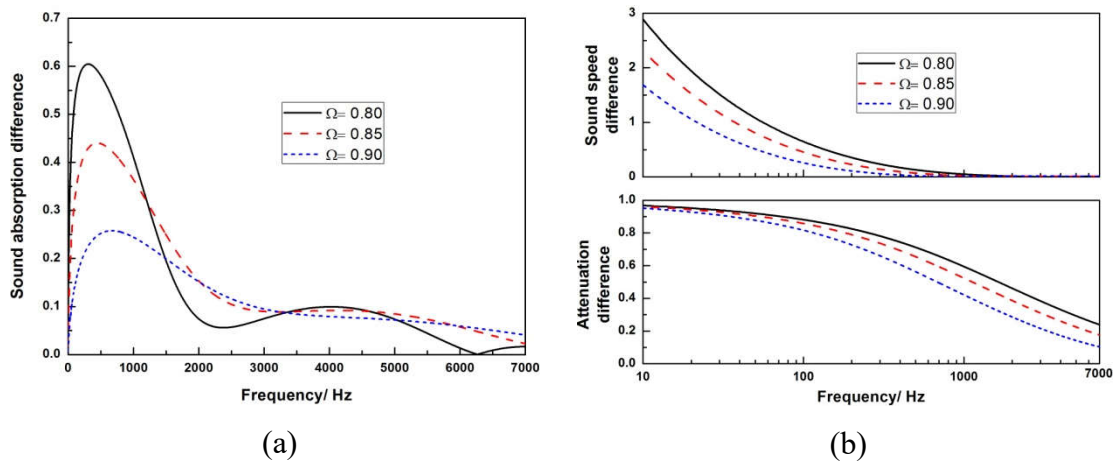

(a)	(b)

Fig. 12 Anisotropic acoustic properties of sintered fibrous metal with different porosities (fiber diameter 50 μm and sheet thickness 20 mm): (a) sound absorption difference; (b) sound speed and attenuation difference

List of table

Table 1. Physical parameters of sintered fibrous metal samples

Physical parameter	Value
Air density	$\rho_0 = 1.29 \ \text{kg/m}^3$
Specific ratio	$\gamma = 1.4$
Prandtl number	$\text{Pr} = 0.702$
Sound speed	$c = 343 \ \text{m/s}$
Kinematic viscosity	$v = 1.46 \times 10^{-5} \ \text{m}^2 / s$
Static pressure of air	$P_0 = 1.0132 \times 10^5 \ \text{Pa}$
Fiber diameter	$a = 50 \ \mu\text{m}$
Porosity	$\Omega = 90\%$